Flexural behavior of HPFRCC: Enhancing post-crack strength and toughness by magnetic alignment of the reinforcement

Igor da Silva Brito, Dimas Alan Strauss Rambo *, Sandro Martini, Renan Pícolo Salvador, Marcos Fabrízio de Menezes Freitas

Department of Civil Engineering, São Judas Tadeu University, 546 Taquari St., 03166-000 São Paulo, Brazil

HIGHLIGHTS

- The magnetic circuit induced fiber overlapping and chain formation in the specimens.
- Fiber orientation resulted in increases of the average UV values for $V_f > 2\%$.
- Fiber orientation resulted in anisotropy on the electrical properties of the HPFRCC.
- Compressive strength, MOR and toughness were improved with aligned fibers.
- Fiber alignment led to a reduction on the critical fiber volume for bending.

GRAPHICAL ABSTRACT
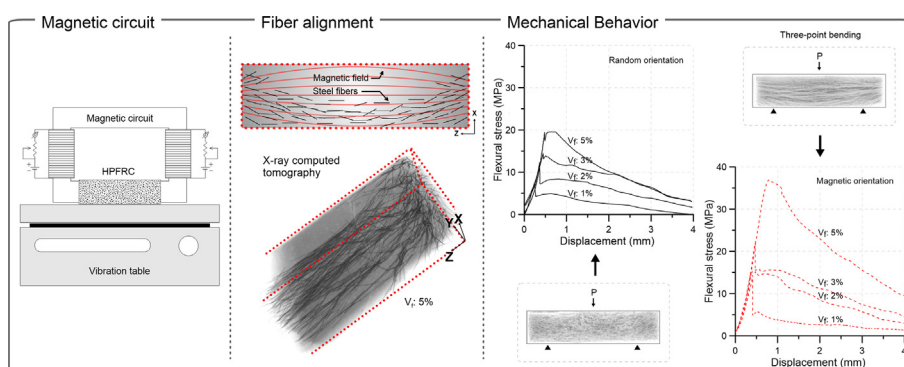
ARTICLE INFO

ABSTRACT

This paper presents an investigation on the effect of magnetic orientation of steel fibers on the physical–mechanical and electrical properties of a High Performance Fiber Reinforced Cement Composite. A simplified magnetic circuit was proposed to align the reinforcement within the cementitious matrix. X-ray Computer Tomography was employed to qualitatively access the fiber distribution in hardened specimens. Physical and electrical properties were characterized by ultrasound propagation velocity and electrical resistivity, while mechanical performance was evaluated by flexural and compressive tests. Scanning electron microscopy was used to study the damage processes in the fiber–matrix interfaces. Results showed that the magnetic circuit designed in this study was able to generate a preferential orientation of the steel fibers, increasing the ultrasound propagation velocity and causing anisotropy in the electrical properties. Furthermore, the modulus of rupture and toughness of the composite were significantly enhanced, leading to a feasible reduction in the critical fiber volume for bending when fibers are aligned.

1. Introduction

The fast-evolving society has continuously demanded a significant effort to develop advanced cement-based materials. High performance fiber reinforced cementitious composites (HPFRCC) have been the subject of several researches, because their tailored and multiple functionalized effectiveness may fulfill the requirements needed for special structural projects [1,30]. The application of these composites must overcome several challenges to achieve the desired fresh and hardened state properties [2,3].

---

* Corresponding author.
   E-mail address: dimasrambo@gmail.com (D. Alan Strauss Rambo).

HPFRCCs are particularly attractive because they may present strain and deflection hardening behavior [4]. Due to the stabilization of crack propagation provided by the fibers, the fracture energy, the load bearing capacity and the pseudo-ductility of the composite are significantly improved. The deformation of HPFRCCs occurs by the formation and opening of multiple microcracks, which reduce considerably the ingress of aggressive agents that may cause detrimental chemical processes and reduce the durability of the element [5,6].

It must be remarked that the critical steel fiber volume needed to achieve that mechanical behavior surpasses 1% (78.5 kg/m^3) [4]. Such amount of fibers may turn handling, casting and finishing operations more complex, since the workability of the fresh mixture may be reduced. Therefore, the matrix may not consolidate properly, and fibers tend to present a random distribution, contributing only partially to the load-bearing capacity of the composite [7].

Constant advancements in techniques to enhance the mechanical properties of HPFRCC are crucial to overcome those concerns. Zhang et al. [8] developed a novel device to cast HPFRCC in layers and align the fibers, which resulted in significant increases of 24% and 66% in first crack strength an ultimate tensile strength, respectively. Huang et al. [9] developed a technique to align steel fibers by controlling the flow and casting directions of fresh HPFRCC, obtaining toughness values 65% higher than concretes with randomly distributed fibers. Moreover, specimens produced by this new casting process were significantly less degraded when exposed to elevated temperatures [10].

Since steel fibers are ferromagnetic materials, they may be magnetically aligned, leading to an optimization crack stress redistribution and to toughness enhancement [11]. By doing so, fiber efficiency may be significantly improved and HPFRCC with lower fiber contents may be obtained. In addition, complementary techniques such as tomography [12], the inductive method [13], X-ray radiography [14] and numerical simulation [15], may be used to detect the quantity, orientation and positioning of the fibers. This accomplishment may turn HPFRCC into a technically and economically competitive material for structural applications, where elements are subjected to unidirectional loads. Patents in this field have been reported in the past focusing on conventional concretes reinforced with steel fibers [16,17]. However, its application is still uncommon in the context of construction engineering.

In this context, this research was proposed to evaluate the influence of magnetic alignment of steel fibers in the physical–mechanical properties of a HPFRCC. A magnetic circuit was developed to align steel fibers within the cementitious matrix. The mechanical properties of HPFRCC containing randomly oriented and magnetically aligned fibers were characterized in terms of compressive strength, flexural strength and toughness. Mechanical properties were correlated with image analysis obtained by X-ray computer tomography and scanning electron microscopy. This analysis was complemented by the determination of ultrasound propagation velocity (UV) and electrical resistivity of each matrix tested. Results showed a considerable enhancement on the mechanical behavior of HPFRCC by fiber alignment and may have a relevant repercussion on the applicability of this composite in structural elements.

2. Experimental methodology

2.1. Design of the magnetic circuit

A magnetic circuit was used to generate a magnetic field capable of aligning steel fibers within a cementitious matrix. This system uses a pair of coils wrapped in a ferromagnetic core to produce a magnetic field. This setup allows magnetizing a specimen through the air gap introduced in the magnetic core.

A scheme of a classic magnetic circuit made of a nucleus (a ferromagnetic material with a regular geometric shape) with a copper wire wrapped-up in its parts is illustrated in Fig. 1-a. In this magnetic system, when an electric current I starts to flow through the coils, a magnetic field H is established in the whole nucleus. The magnetic vector field $\vec{H}$ may be expressed by using Ampèrés law for magnetic materials, presented in equation (1).

$$\oint_C \vec{H} . d\vec{\ell} = I \tag{1}$$

where $d\vec{\ell}$ is an infinitesimal oriented element of the curve C.

For the nucleus in Fig. 1-a, equation (2) may be applied

$$H = \frac{(N_1 + N_2)I}{\ell} \tag{2}$$

with N_1 and N_2 representing the number of turns in coil 1 and 2, respectively, and ℓ the length considering the center of the nucleus.

Thus, considering that the nucleus has a relative magnetic permeability μ_r, the magnetic flux density B is given by equation (3).

$$B = \mu_0 \mu_r H = \frac{\mu_0 \mu_r (N_1 + N_2)I}{\ell} \tag{3}$$

where μ_0 represents the magnetic permeability of vacuum ($\mu_0 = 4\pi \times 10^{-7}$ Tm/A).

It is possible to observe that the magnetic field is a function of the number of turns, current, and the relative magnetic permeability of the nucleus material. Equation (3) may be rewritten in terms
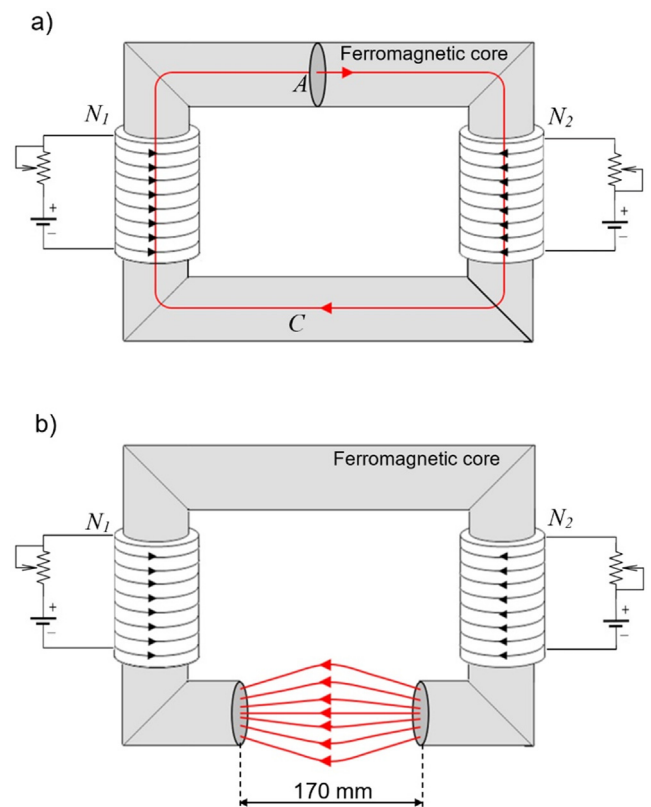

Fig. 1. Scheme of a magnetic circuit: (a) containing two coils (N1 e N2) and a ferromagnetic material as nucleus with a cross section A (red line represents the magnetic flux); (b) with the air gap containing two coils and a ferromagnetic material as nucleus (red lines represent the spreading of the magnetic flux). (For interpretation of the references to colour in this figure legend, the reader is referred to the web version of this article.)

of the magnetic flux (ϕ_M). Assuming a uniform magnetic field normal to the section area A, the flux is given by equation (4).

$$\phi_M = BA = \frac{\mu_0 \mu_r A (N_1 + N_2) I}{\ell} \qquad (4)$$

With the information provided, a magnetic circuit represented in Fig. 1-b was developed to align fibers in the HPFRCC matrix. It was necessary to introduce an air gap on the original circuit system to spread the magnetic flux through the air gap edges. Based on the physical foundations, the orientation setup consists of two copper wire coils with 2.5 mm diameter, and 126 turns around the silicon-steel core. Therefore, the magnetic flux density possesses the north and south poles on the edge of the core.

A power supply with 12 V output voltage and a maximum current of 16 A were used to establish the electric current in the coils. The rheostats were used to control the electric current intensity (registered using multimeters). A magnetic flux density of 9.5×10^{-3} T is obtained at the air gap edges when a current of 12 A circulates in each of the coils.

2.2. Materials

The cementitious materials employed to produce the composites were a commercially available high-early strength Portland cement (CEM I 52.5R), silica fume (920U from Elkem Co.) and metakaolin (Metacaulim HP ULTRA from Metacaulim do Brasil Co.). The choice of using two pozzolans was based on particle sizes, seeking to improve the packing density of the mixture. Table 1 summarizes the physical and chemical properties of the cement, silica fume and metakaolin.

A quartz sand (Brasilminas Co.) with particle size distribution ranging from 0.075 mm to 2 mm was used as aggregate. A polycarboxylate superplasticizer (Adiment Premium from Vedacit Co.) with 30% of solid content was employed to provide adequate workability to favor magnetic alignment of the reinforcement within the matrix. The water/cementitious material ratio of the matrices was kept at 0.3.

The composites produced in this study were reinforced with short straight steel fibers (from Astra Co.) with tensile strength of 1100 MPa, elastic modulus of 210 GPa and specific weight equal to 7850 kg/m^3. The length, diameter and aspect ratio of the fibers were 12.5 mm, 0.5 mm and 25, respectively. According to the Brazilian standard ABNT NBR 15530:2007, such fibers are classified as R-I (type-class).

2.3. Composition and preparation of the cementitious matrix

Five mixtures were produced in this study and their composition is presented in Table 2. One of them was the control mixture (M0), which did not contain steel fibers, and the additional four mixtures contained fiber volume fractions equal to 1%, 2%, 3% and 5% (M1, M2, M3 and M5, respectively). The inclusion of fibers in the composites was performed by replacing the volume of the matrix with the corresponding volume of fibers. For comparative

purposes, mixtures containing fibers were produced with random (RA) and aligned (AL) reinforcement. The nomenclature adopted to identify the mixtures is 'Mfiber volume'_'spatial arrangement of fibers'.

The following mixing procedure was conducted for the HPFRCC production: first all anhydrous binders were mixed in a planetary mixer during 1 min at low speed (rotational and planetary speed equal to 140 and 62 rpm, respectively). Then 2/3 of the water and 2/3 of the superplasticizer were added and mixed for 2 min at high speed (rotational and planetary speed equal to 285 and 125 rpm, respectively). Subsequently, aggregates were added and mixed for 1 min at low speed and additional 30 s at high speed. The addition of the remaining portion of water superplasticizer and steel fibers (when necessary) was conducted during 1 min at low speed. Finally, a blend of 1 min at low speed was employed to conclude the mixing process.

The workability of the mixtures was evaluated according to the standard [18]. The spread diameter of M0, M1, M2, M3 and M5 was, respectively, 390 mm, 340 mm, 321 mm, 365 mm and 385 mm, with no bleeding nor segregation. After the characterization of the fresh state properties, prismatic specimens for each mixture (RA and AL) listed in Table 2 were produced.

2.4. Specimen preparation

The alignment of steel fibers within the matrix (mixtures AL) was conducted using the magnetic circuit presented in Fig. 1.b. The fresh cementitious matrix containing steel fibers was cast into acrylic molds measuring 40 mm × 40 mm × 160 mm (width × height × length). The casting process was carried out from the center of the molds leaving the mixtures free to flow towards the ends. After casting, molds were placed on a vibration table and positioned in the air gap of the circuit (see Fig. 1). Right after that, vibration (60 Hz) and magnetic field were simultaneously applied during 40 s. The magnetic field was used to control fiber orientation, in order to generate an adequate magnetic torque to align fibers. The magnetic field was generated with an electric current equal to 12 A, which was adopted based on preliminary experiments performed by the authors [19].

Once the alignment process was completed, molds were removed from the magnetic circuit and stored in a cure chamber with 100% RH and 23 ± 1 °C for 24 h. Specimens were demolded and subjected to thermal curing in lime-saturated water, at 53 °C (+/- 2 °C) for 14 days. After this period, the specimens were removed from the humid chamber and left in room humidity and temperature for 24 h before the characterization of mechanical and electrical properties.

2.5. Test methods

Table 3 summarizes the tests performed with the HPFRCC. All the tests were performed at the age of 16 days. Their descriptions are presented in sections 2.5.1 to 2.5.6.

Table 1
Physical and chemical properties of the cement, silica fume and metakaolin.

		Cement	Silica fume	Metakaolin
Physical properties	Density (g/cm^3)	3.10	2.20	2.56
	Size range (μm)	0.2–80	0.015–1	0.1–50
Chemical composition (%)	Al$_2$O$_3$	5.2	0.4	34.0
	CaO	63.3	0.2	0.1
	SiO$_2$	19.2	97.5	57.0
	Fe$_2$O$_3$	2.8	0.1	2.0
	SO$_3$	2.8	0.1	0.1
	Others	6.7	1.7	6.8

Table 2
Mix composition of the cementitious matrices analyzed.

Constituent (kg/m^3)	Mixtures				
	M0	M1	M2	M3	M5
Cement	599.2	593.2	587.2	581.2	569.2
Metakaolin	257.6	255.1	252.5	249.9	244.7
Silica fume	65.9	65.2	64.6	63.9	62.6
Sand	1315	1302	1289	1276	1064
Water	179.7	177.9	176.1	174.3	170.7
Short straight steel fiber	0	78.5	157	235.5	392.5
Superplasticizer	25.7	25.5	25.2	24.9	24.4

Table 3
Tests performed with the HPFRCC.

Test	Specimen	Reference
X-ray computed tomography	Broken halves of prismatic specimens	[20]
Ultrasound propagation velocity	Prismatic specimen	[21]
Electrical resistivity	Prismatic specimen	[22]
Three-point bending test	Prismatic specimen	[23]
Scanning electron microscopy	Slices of fractured prismatic specimen	[24]
Compressive strength test	Broken halves of prismatic specimens	[23]

2.5.1. X-ray computed tomography

X-ray computed tomography (XCT) was performed in hardened specimens of the composite M5_AL to assess the distribution and positioning of steel fibers along its volume. Specimens measuring 70 mm × 40 mm × 13 mm (length × height × thickness) fixed in styrofoam cubes were used for this test. XCT imaging was conducted in a Carl Zeiss tomograph model METROTOM 800 (130 kV). A current of 200 μA was employed while the integration point, Voxel and spot were equal to 500 ms, 56,06 μm and 40 μm, respectively. The 360° rotation images were then reconstructed to obtain the 3D volume.

2.5.2. Ultrasound propagation velocity

Ultrasound propagation velocity (UV) was determined longitudinally in all prismatic specimens (three per mixture) produced for flexural tests. The equipment used was a model Pundit Lab, from PROCEQ Co, coupled to 54 kHz transducers. Ultrasound propagation velocity was calculated by the distance between the transducers divided by the propagation time.

2.5.3. Electrical resistivity

The equipment used for the test was the Resipod from PROCEQ Co, in the range from 1 kΩcm to 1000 kΩcm using a frequency of 40 Hz. This model has a probe size of 5 mm. The probes are equally spaced 50 mm apart. Therefore, the inner probes have a 50 mm spacing, and the outer probes have a spacing of 150 mm. The equipment operates according to the principle of the Wenner device [22]. A current is applied between the external probes, and the potential difference is measured between the internal ones. The resistivity obtained depends on the electrical properties of the material and on the spacing of the probes. The electrical resistivity was measured in all faces of the specimens (three per mixture) produced for flexural tests.

2.5.4. Three-point bending test

All HPFRCC specimens were subjected to three-point bending test at the age of 16 days. Tests were performed in a Kratos universal testing machine, model KE 20000MP, coupled to a 200 kN load cell. Prismatic specimens were supported by two steel cylinders (Ø 10 mm) 100 mm distant from each other. Specimens were loaded at midspan by another steel cylinder (Ø 10 mm) at a rate equal to 0.5 mm/min until the total displacement of 4 mm was reached. Load application rate was controlled by the actuator displacement (linear variable differential transducers were not employed).

Before the test, all specimens were rotated 90° in relation to the casting direction. This procedure ensures flatness in load application areas and points of support. Flexural stresses were calculated according to equation (5):

$$\sigma_F = \frac{1.5PL}{40^3} \tag{5}$$

where σ_F is the flexural stress (MPa), P is the load applied vertically to the prism (N) and L is the distance between the supports (mm).

The toughness of all composites subjected to the three-point bending test was calculated as the total area under the load–displacement curve up to 4 mm.

2.5.5. Scanning electron microscopy

Once the three-point bending tests were performed, the fiber–matrix interfaces of the HPFRCC were investigated using scanning electron microscopy (SEM). The equipment employed for the analyses was a FEI Quanta 250. Thin slices (~7 mm) of the fractured area of the prisms subjected to bending (40 mm × 40 mm) were dry cut with a precision saw and coated with 20 nm of gold to become conductive and suitable for conventional SEM analysis. The microscope was operated using 25 kV of acceleration tension and about 30 mm of working distance. The analyzed face was the fractured face of the prisms.

2.5.6. Compression test

The uniaxial compressive strength of the HPFRCC was determined on halves of the prisms derived from three-point bending tests (six specimens for each mixture produced). Despite the high fiber contents used in the composites, manual separation of the halves of the prisms was possible due to the geometry and reduced length of the fibers. The compressive strength test employs a rigid jig coupled to the testing machine to transmit the loads to the surface of the HPFRCC specimen (40 mm × 40 mm). The same load cell and actuator displacement rate employed for the bending test (see item 2.5.4) were used for the compression tests. The compressive stress was calculated by dividing the maximum load at fracture by the area of the platens (1600 mm^2). Similarly to the flexural test, all specimens were rotated 90° in relation to the casting direction before loading.

3. Results and discussion

3.1. Influence of magnetic alignment on fiber distribution

Fig. 2 illustrates the distribution of the fibers along the volume of a M5_AL specimen after exposure to the magnetic field and vibration. It is possible to observe that the distribution of fibers
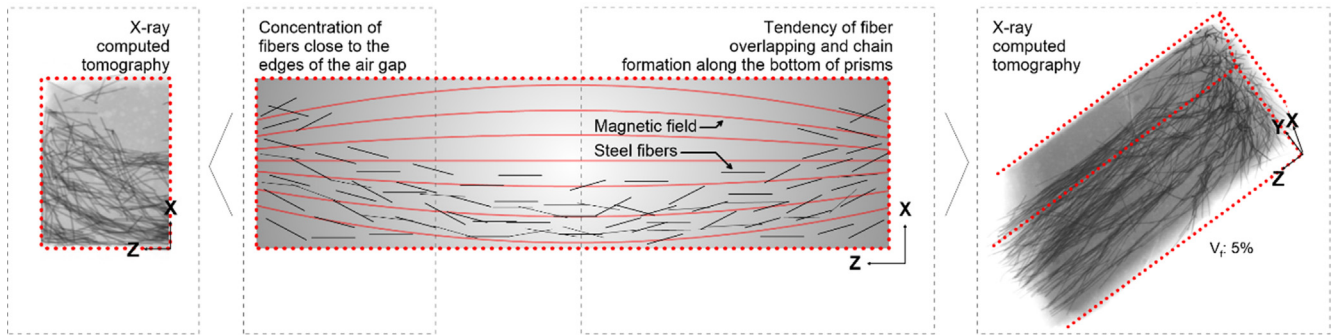
Fig. 2. XCT images and simplified scheme of the fiber positioning along the volume of prisms.

within the specimen is not uniform. As expected, fibers remained aligned in the direction of the magnetic flux. However, a clear concentration of fibers close to the edges of the air gap (point of maximum intensity of the magnetic field) and in the lower third of the specimen (bottom face) is observed. Since both fiber concentration points are important and affect the mechanical behavior of HPFRCC in different ways, it will be discussed separately in the sequence.

When using a magnetic circuit combined with vibration of the molds, fibers tend to align following the direction of the magnetic flux just in front of the ends of the air gap, where intensity is $9,5 \times 10^{-3}$ T [19,22]. In this portion of the specimens, which is subjected to compression tests, gravity action is not capable to move the fibers to the bottom, which explains the large amount of fibers adhered to the face closest to the circuit (Fig. 2).

Fiber concentration at the bottom of the molds occurs in part due to the dipole–dipole interactions of the reinforcement [16]. The fibers under the action of the magnetic flux are magnetized, and may be considered as magnets, magnetic dipoles, which tend to align with the magnetic flux and suffer an attraction or repulsion among themselves. Such process results in a tendency of fiber overlapping and chain formation. As fibers are 3 times denser than the matrix, fiber magnetization allied to the gravity action, vibration process and wall effect, leads the fibers to the bottom of the molds. As reported by Alberti et al. [25], fresh-state properties, consolidation procedures and wall effects are among the main sources of anisotropy which affect fiber positioning and, consequently, the mechanical response of fiber reinforced composites.

3.2. Determination of the ultrasound propagation velocity of HPFRCC

Fig. 3 shows the results of the UV along the longitudinal direction for both RA and AL mixtures. Comparing M1, M2, M3 and M5 with M0, it is possible to note that the inclusion of steel fibers results in increases of the longitudinal UV. This behavior occurs because fibers act as wave propagation guides, since ultrasound propagation by metallic medium occurs around 27% faster (~5900 m/s) [26] than in the cementitious matrix employed in this study (4652 m/s). In addition, once the fibers are aligned along the longitudinal direction of the specimen, the wave transmission occurs more efficiently, resulting in further increases of the UV average values.

Increases in UV in specimens with aligned fibers were observed in M2, M3 and M5. Mixtures M2_AL, M3_AL and M5_AL presented increases of the UV equal to 8%, 4% and 2%, respectively, when compared to the random peers. The tendency for smaller differences in UV values between AL and RA with increasing fiber volume results from the lower distance between individual fibers and greater volume of steel used in the composites with larger amount of fibers (e.g.: 5%).
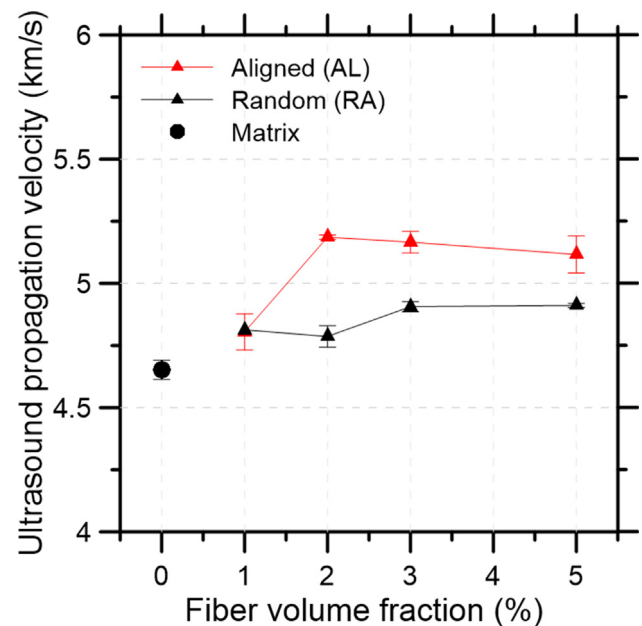

Fig. 3. Average ultrasound propagation velocity measured longitudinally in all mixtures produced.

Mixtures M1_RA and M1_AL presented similar values due to the low volume of steel employed in these composites. Besides, by decreasing the fiber volume, the distance between individual fibers increases. This distancing prevents fiber overlapping when the reinforcement is oriented, leading to reductions in the ultrasound propagation velocity.

3.3. Determination of the electrical resistivity of HPFRCC

Fig. 4 depicts the results of the electrical resistivity of random (Fig. 4-a) and aligned (Fig. 4-b) mixtures as a function of the specimen faces. A trend of reduction of the electrical resistivity with the magnetic alignment is observed.

Specimens containing randomly oriented fibers present statistically equal values of electrical resistivity in all specimen faces (Fig. 4-a). Such isotropic characteristic demonstrates a uniform fiber distribution along the prismatic specimens containing 1%, 2%, 3% and 5% of fibers. In these specimens, a trend of reduction of the electrical resistivity with increasing fiber volume was observed. The only exception is the mixture M3_RA, which presents statistically equal values of electrical resistivity to those observed for M2_RA (considering the averages of the four faces as group of samples).
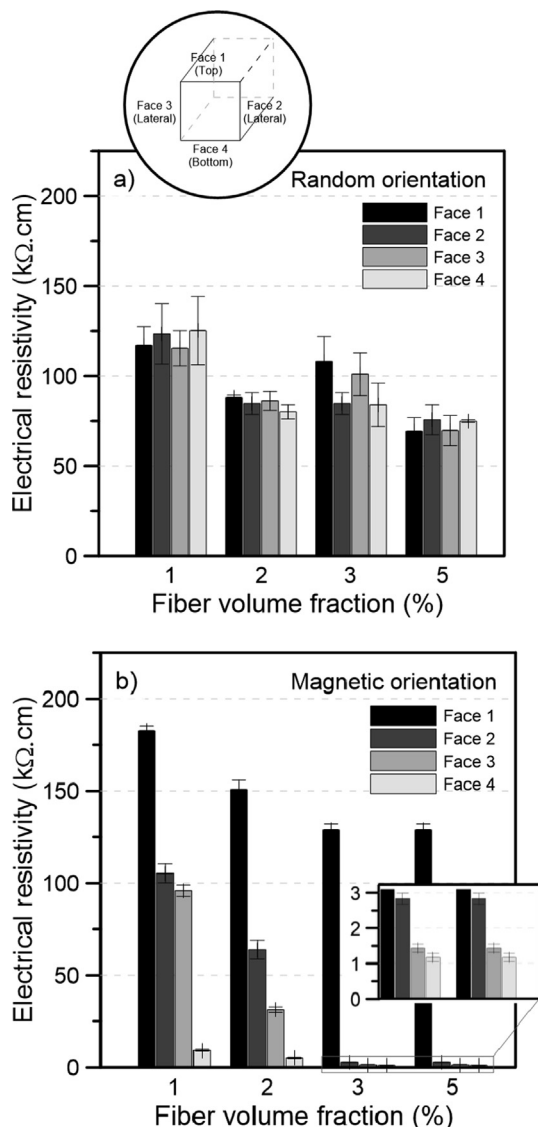
Fig. 4. Electrical resistivity as a function of the faces of the specimens: (a) random orientation and (b) magnetic orientation.

Specimens containing aligned fibers present the opposite behavior (Fig. 4-b), and significant resistivity reductions are observed for the side and bottom faces of the specimen, which are regions with higher concentrations of fibers (Fig. 2). As the top face of the specimen has few fibers (see Fig. 2), the electric current is transported only by the ions in the matrix pore solution, increasing its electrical resistivity. The bottom face has the highest amount of fibers, as evidenced by XCT images (Fig. 2). This is due to the dipole–dipole interactions that promote fiber agglomeration, leading the fibers to the bottom of the molds, as mentioned in 3.1. In this situation, the bottom face is rich in metallic fibers, which reduces its electrical resistivity and makes it more conductive than the other faces.

3.4. Flexural behavior of HPFRCC

Fig. 5 shows typical stress–displacement curves obtained from the flexural tests grouped by fiber content. The red dashed curves represent the flexural behavior of mixtures with aligned fibers (mixtures AL). The continuous black curves represent the specimens with randomly oriented fibers (mixtures RA). The curves

obtained indicate a deflection softening behavior for the mixtures M1_RA, M1_AL, M2_RA, M2_AL and M3_RA. All other composites presented a deflection hardening behavior.

Table 4 presents the average results of modulus of rupture (MOR) and toughness up to 4 mm displacement. As may be observed, the flexural performance in terms of MOR and toughness are higher in mixtures AL than in mixtures RA for all the fiber contents evaluated. This behavior was more pronounced for the composite M5_AL, which presented increases of MOR and toughness of, respectively, 72.6% and 114.6% in comparison to the M5_RA. It is likely that, in the case of the mixture M1_RA, the incorporation of random fibers has impaired the matrix compaction, generating MOR values lower than those observed for M0. It is also important to remark that fiber orientation was capable to reduce the critical fiber volume for bending, which may be clearly observed on Fig. 5-c.

These large increments obtained with magnetic alignment reflect the preferential orientation of the reinforcement, as well as the fiber concentration in part of the tensioned region of the prisms, previously discussed in the item 3.1. It is important to remark that specimens were rotated 90° in relation to the casting direction before the bending tests. That is why the emphatic note that the fibers are deposited in part of the tensioned region of the prisms.

Conventional SEM analysis performed on fractured prisms showed that in mixtures RA, fibers inclined with respect to the loading direction generated matrix damage (or spalling) in their surroundings (Fig. 6-a). According to [27–29], such process reduces the extension of the fiber–matrix interface as well as the pull-out length, limiting the potential load bearing capacity of the composite. This trend is in total agreement with the lower toughness values observed for mixtures RA presented in Table 4.

In addition, Fig. 6 revealed that the failure mode of the RA specimens occurred with the pull-out of the reinforcement, that is, without fiber breakage (see the preserved fiber tip in Fig. 6-a). Such behavior results from the length of the fibers (12.5 mm) which is below the critical value (~30 mm) necessary to promote its rupture. This finding is important since it excludes the idea that the reduction of MOR and toughness in the RA prisms may be associated with the abrupt rupture of the reinforcement, sometimes common for inclined fibers [27–29].

Fig. 7 presents the Hoerl fitting to correlate toughness with the fiber volume employed for the HPFRCC production [30]. It is possible to observe that the magnetic alignment leads to a remarkable reduction in the fiber volume necessary to reach a certain value of toughness. For example, using 2% and 3% of random fibers, toughness values of around 9.5 J and 13.2 J are obtained (see Table 4). In the case of specimens with aligned reinforcement, same toughness values are obtained with around 1.7% and 2.2% of fibers respectively, reducing the need of V_f in 15% and 26%.

Another interesting point is that the toughness enhancement for an increase of 1% in fiber volume is significantly different depending on the orientation method. Comparing the average toughness gain between the M2 and M3 for both cases, RA and AL (Table 4), is it possible to note values practically 30% grater for the AL case. This fact results from the greater amount of fibers crossing the fractured section in the AL case. Studies reported by Abrishambaf et al. [31] show that for composites reinforced with 3% of steel fibers (AL and RA), the amount of fibers / cm^2 in the fractured section of the specimens can be almost 50% higher in the case of oriented fibers.

It is believed that the greater distance between the toughness fitting lines RA and AL for higher fiber volumes of 3% and 5% is directly related to the dipole–dipole interactions discussed previously in the section 3.1. As reported by Wijjffels et al. [12], the shorter the distance between the fibers, the greater the tendency
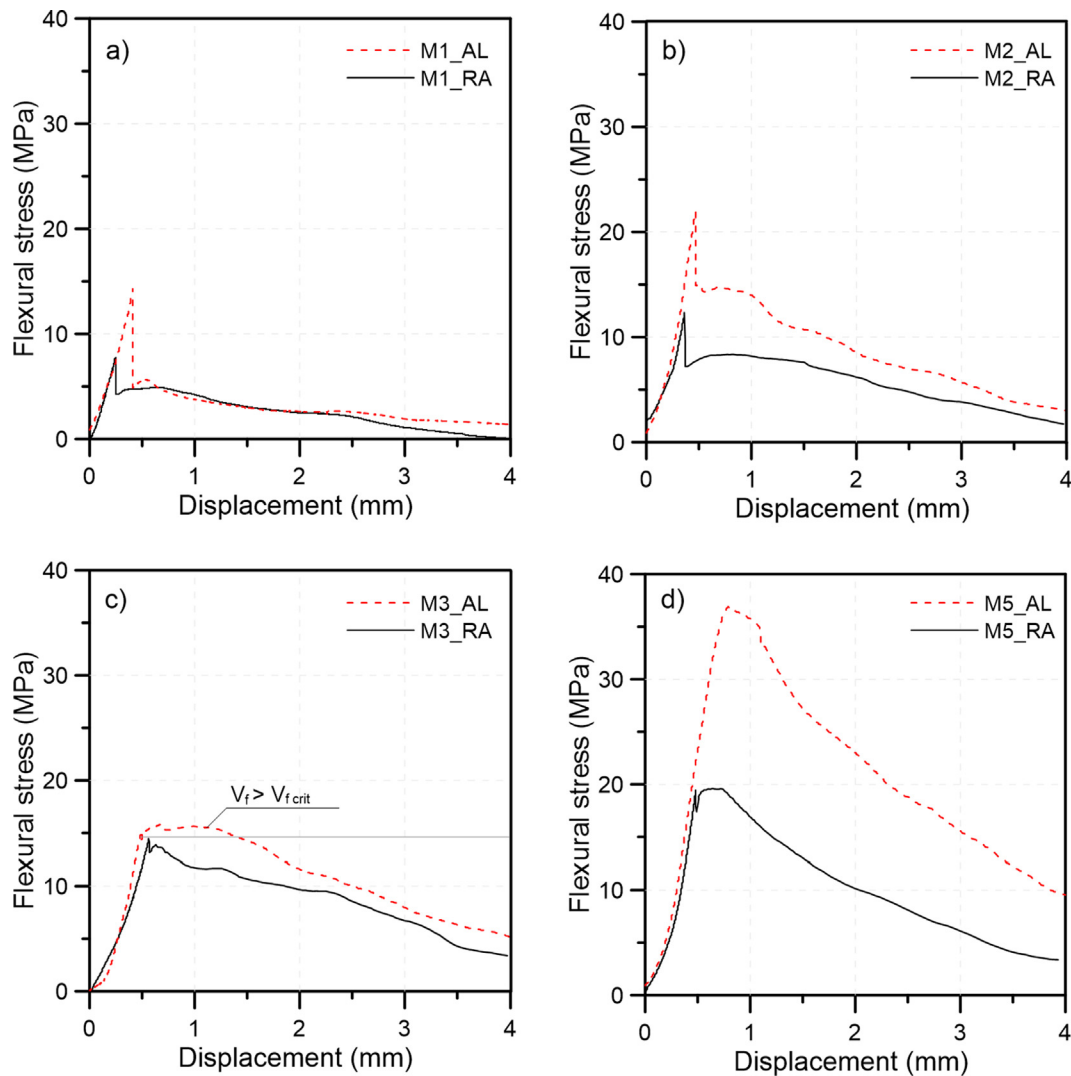
Fig. 5. Typical stress-displacement curves for HPFRCC specimens reinforced with 1% (a), 2% (b), 3% (c) and 5% (d) of fibers (AL and RA).

Table 4
Mean values and standard deviation of MOR and toughness (up to 4 mm displacement) obtained for the HPFRCC beams subjected to flexural tests.

Mixture	MOR(MPa)	Δ MOR*(%)	Toughness**(J)	Δ Toughness***(%)
M0	15.5 ± 3.5		1.5 ± 0.3	
M1_AL	15.8 ± 0.9	+71.7	4.0 ± 2.0	+2.6
M1_RA	9.2 ± 0.6		3.9 ± 0.7	
M2_AL	21.7 ± 0.8	+22.6	14.2 ± 0.5	+40.6
M2_RA	17.7 ± 0.4		10.1 ± 2.0	
M3_AL	17.1 ± 1.7	+5.6	17.5 ± 2.4	+37.8
M3_RA	16.2 ± 0.3		12.7 ± 0.9	
M5_AL	36.6 ± 0.8	+72.6	33.7 ± 0.2	+114.6
M5_RA	21.2 ± 1.0		15.7 ± 0.7	

*Variation of MOR between composites AL and RA.
**Toughness determined from the area under the curve from 0 to 4 mm
***Variation of accumulated toughness between composites AL and RA.

of fiber overlapping and chain formation due to the dipole–dipole interactions. Therefore, higher concentrations of fibers will result in more fiber chains (i.e.: increased orientation factor), decreasing the randomness of the reinforcement and consequently increasing toughness. The increases in the ultrasound propagation velocity and the reductions of the electrical resistivity in the AL specimens confirm these observations.

3.5. Compressive strength of HPFRCC

Fig. 8 presents the compressive strength of the HPFRCC mixtures determined at 16 days. Average results obtained from the six cubic specimens are given in Table 5. Similarly to flexural tests, the inclusion of fibers provided improvements on the HPFRCC compressive strength. Mixtures M1_RA, M2_RA, M3_RA and
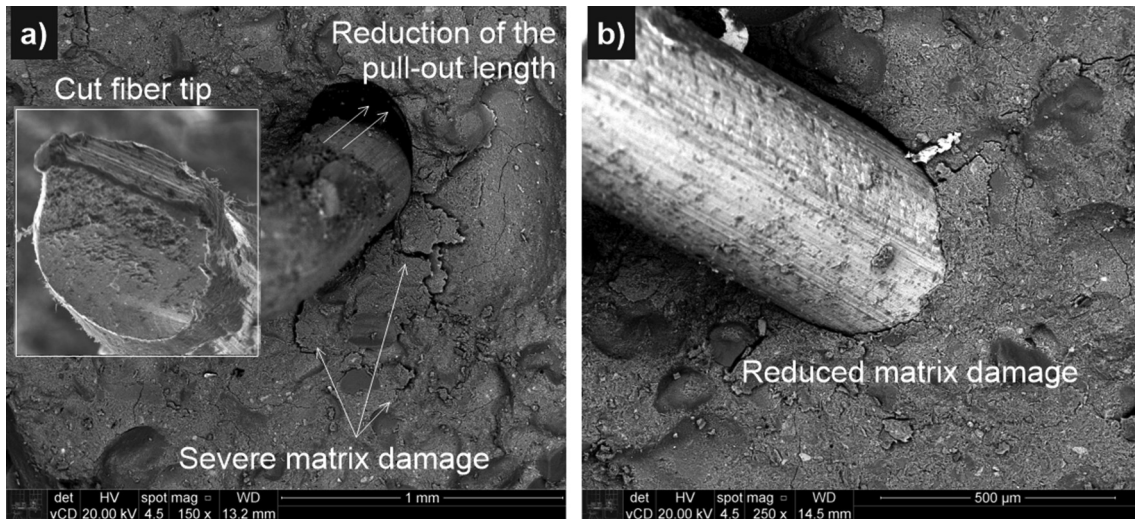
Fig. 6. SEM micrographs performed on fractured prisms with (a) inclined fibers (RA case) and (b) aligned fibers (AL case).
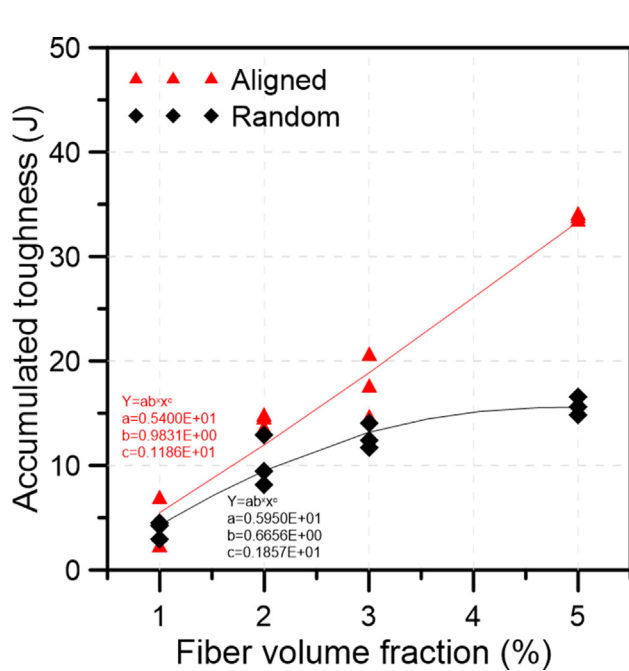

Fig. 7. Relation between accumulated flexural toughness and fiber volume fraction for HPFRCC.

Fig. 8. Relation between compressive strength and fiber volume fraction for HPFRCC.

M5_RA presented the respective compressive strength values of 4.9%, 14.6%, 21% and 36.4% higher than those obtained for M0. Due to fiber alignment, the increases in compressive strength were greater, reaching 8.3%, 23.6%, 30.8% and 44.7% in mixtures M1_AL, M2_AL, M3_AL and M5_AL, respectively.

Specimens subjected to magnetic alignment presented compressive strength values 6 to 10% higher than specimens with randomly oriented fibers. Such distinct effect occurs due to the orientation phenomenon associated with the concentration of fibers at the specimen extremities (in front of the ends of the air gap), where the compressive strength was determined. As previously discussed in the item 3.1, this process results in large amounts of fibers intersecting the fractured sections of the AL specimens, increasing compressive strength of these composites. It is important to emphasize that, the concentration of fibers at
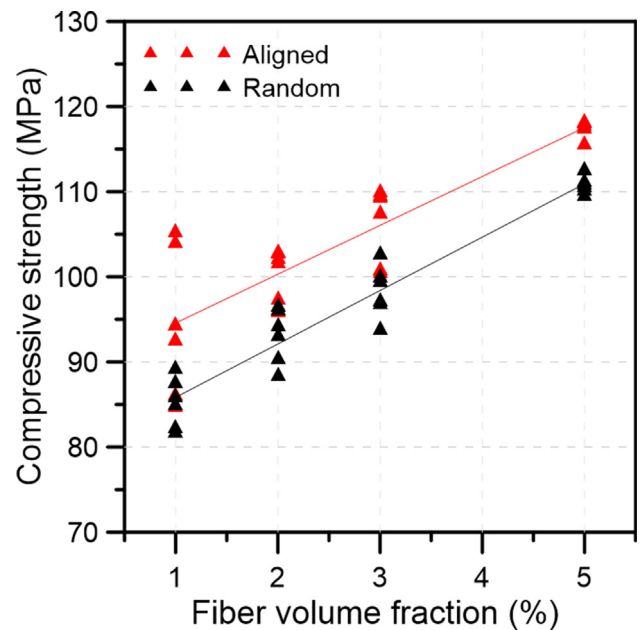
Table 5
Average values and standard deviation of compressive strength obtained for the HPFRCC cubes under compression.

Mixture	Compressive strength (MPa)
M0	81.2 ± 2.8
M1_AL	94.4 ± 7.9
M1_RA	85.2 ± 2.7
M2_AL	100.4 ± 2.8
M2_RA	93.1 ± 2.9
M3_AL	106.2 ± 4.0
M3_RA	98.2 ± 2.8
M5_AL	117.4 ± 0.9
M5_RA	110.8 ± 0.9

the ends of the specimens as well as their small size, make the results not representative for HPFRCC with the indicated fiber volumes.

4. Conclusions

The following conclusions may be drawn from the experimental campaign conducted:

- The designed magnetic circuit was capable to generate a preferential orientation of steel fibers within the high performance matrix employed in this study.
- The dipole–dipole interactions stablished between steel fibers resulted in fiber overlapping and chain formation along the bottom face of the specimens. In addition, a clear concentration of fibers occurred close to the edges of the air gap (point of maximum intensity of the magnetic field). The XCT analyses confirm these observations.
- The orientation of fibers along the length of the prismatic specimens resulted in increases of the UV average values for all HPFRCC with fiber volumes above 2%.
- As evidenced by the XCT analysis, the concentration of fibers at the extremities and bottom of the specimens containing aligned fibers resulted in a trend of reduction of the electrical resistivity on their side and top faces. However, the RA specimens presented isotropic characteristics, once similar values of electrical resistivity were obtained in all faces evaluated.
- The magnetic orientation of the fibers improved the compressive strength, MOR and toughness of the HPFRCC for all fiber volume fractions studied. Both increments were more pronounced for the mixture containing 5% of aligned fibers.
- Fiber alignment was capable to reduce the critical fiber volume for bending. The stress-displacement curves obtained for the composites containing 3% of random and aligned fibers confirm this observation.
- Obviously, the magnetic alignment of steel fibers can benefit the tensile performance of the concrete. It is believed that this technique has a great future in the production of structural elements, especially thin ones, whose production employs mechanical vibration (e.g.: tunnel segments, pipes and precast elements). It is also believed that the advancement of the technique will depend on the use of new methodologies adaptable to traditional methods of construction.

CRediT authorship contribution statement

Igor Silva Brito: Data curation, Investigation, Methodology. **Dimas Alan Strauss Rambo:** Conceptualization, Formal analysis, Software, Supervision, Writing - original draft. **Sandro Martini:** Project administration, Resources, Validation, Visualization, Formal analysis. **Renan Pícolo Salvador:** Formal analysis, Writing - review & editing. **Marcos Fabrízio de Menezes Freitas:** Investigation.

Declaration of Competing Interest

The authors declare that they have no known competing financial interests or personal relationships that could have appeared to influence the work reported in this paper.

Acknowledgements

References

[1] A.E. Naaman, H. Hammoud, Fatigue characteristics of high performance fiber-reinforced concrete, Cem. Concr. Compos. 20 (1998) 353–363, https://doi.org/10.1016/S0958-9465(98)00004-3.

[2] M. Foglar, R. Hajek, J. Fladr, J. Pachman, J. Stoller, Full-scale experimental testing of the blast resistance of HPFRCC and UHPFRCC bridge decks, Constr. Build. Mater. 145 (2017) 588–601, https://doi.org/10.1016/j.conbuildmat.2017.04.054.

[3] T. Ayub, N. Shafiq, M. Fadhil Nuruddin, Mechanical properties of high performance concrete reinforced with basalt fibers, Procedia Eng. 77 (2014) 131–139, https://doi.org/10.1016/j.proeng.2014.07.029.

[4] A.E. Naaman, J.R. Homrich, Tensile stress strain properties of SIFCON. ACI Mater. J.

[5] C. Meng, W. Li, L. Cai, X. Shi, C. Jiang, Experimental research on durability of high-performance synthetic fibers reinforced concrete: Resistance to sulfate attack and freezing-thawing, Constr. Build. Mater. 262 (2020) 120055, https://doi.org/10.1016/j.conbuildmat.2020.120055.

[6] L. Feo, F. Ascione, R. Penna, D. Lau, M. Lamberti, An experimental investigation on freezing and thawing durability of high performance fiber reinforced concrete (HPFRC), Compos. Struct. 234 (2020) 111673, https://doi.org/10.1016/j.compstruct.2019.111673.

[7] S. Zhang, C. Zhang, L. Liao, Investigation on the relationship between the steel fibre distribution and the post-cracking behaviour of SFRC, Constr. Build. Mater. 200 (2019) 539–550, https://doi.org/10.1016/j.conbuildmat.2018.12.081.

[8] Y. Zhang, Y. Zhu, S. Qu, A. Kumar, X. Shao, Improvement of flexural and tensile strength of layered-casting UHPC with aligned steel fibers, Constr. Build. Mater. 251 (2020) 118893, https://doi.org/10.1016/j.conbuildmat.2020.118893.

[9] H. Huang, X. Gao, L. Li, H. Wang, Improvement effect of steel fiber orientation control on mechanical performance of UHPC, Constr. Build. Mater. 188 (2018) 709–721, https://doi.org/10.1016/j.conbuildmat.2018.08.146.

[10] H. Huang, R. Wang, X. Gao, Improvement effect of fiber alignment on resistance to elevated temperature of ultra-high performance concrete, Compos. Part B Eng. 177 (2019) 107454, https://doi.org/10.1016/j.compositesb.2019.107454.

[11] R. Mu, H. Li, L. Qing, J. Lin, Q. Zhao, Aligning steel fibers in cement mortar using electro-magnetic field, Constr. Build. Mater. 131 (2017) 309–316, https://doi.org/10.1016/j.conbuildmat.2016.11.081.

[12] M.J.H. Wijffels, R.J.M. Wolfs, A.S.J. Suiker, T.A.M. Salet, Magnetic orientation of steel fibres in self-compacting concrete beams: Effect on failure behaviour, Cem. Concr. Compos. 80 (2017) 342–355, https://doi.org/10.1016/j.cemconcomp.2017.04.005.

[13] I. Galobardes, C.L. Silva, A. Figueiredo, S.H.P. Cavalaro, C.I. Goodier, Alternative quality control of steel fibre reinforced sprayed concrete (SFRSC), Constr. Build. Mater. 223 (2019) 1008–1015, https://doi.org/10.1016/j.conbuildmat.2019.08.003.

[14] R.A. Raju, S. Lim, M. Akiyama, T. Kageyama, Effects of concrete flow on the distribution and orientation of fibers and flexural behavior of steel fiber-reinforced self-compacting concrete beams, Constr. Build. Mater. 262 (2020) 119963, https://doi.org/10.1016/j.conbuildmat.2020.119963.

[15] V.P. Villar, N.F. Medina, F. Hernández-Olivares, A model about dynamic parameters through magnetic fields during the alignment of steel fibres reinforcing cementitious composites, Constr. Build. Mater. 201 (2019) 340–349, https://doi.org/10.1016/j.conbuildmat.2018.12.105.

[16] A.I. Miller, F.R. Björklund, inventors; Institute for Innovationsteknik AB, assignee. 1975-07-17. Method of Reinforcing Concrete with Fibres, US Patent 4062913A.

[17] B. Svedberg, inventor. Method and device for magnetic alignment of fibres, 1998-06-24.

[18] ABNT NBR 13276. Mortars applied on walls and ceilings - Determination of the consistence index, 2016.

[19] I.S. Brito, Compósito cimentício de alto desempenho reforçado com fibras de aço alinhadas por meio de campo magnético. Master dissertation. Universidade São Judas Tadeu, 2019.

[20] J. Kastner, B. Plank, A. Reh, D. Salaberger, C. Heinzl, Advanced X-Ray Tomographic Methods for Quantitative Characterisation of Carbon Fibre Reinforced Polymers, in: 4th Int. Symp. NDT Aerosp., 2012.

[21] ABNT NBR 8802. Hardened concrete - Determination of ultrasonic wave transmission velocity, 2019.

[22] K.R. Gowers, S.G. Millard, Measurement of concrete resistivity for assessment of corrosion severity of steel using wenner technique, ACI Mater. J. v. 96, n.5 (1999) 536–541.

[23] ABNT NBR 13279:2005. Mortars applied on walls and ceilings - Determination of the flexural and the compressive strength in the hardened stage.

[24] D.A.S. Rambo, F. de Andrade Silva, R.D. Toledo Filho, O. da Fonseca Martins Gomes, Effect of elevated temperatures on the mechanical behavior of basalt

textile reinforced refractory concrete, Mater. Des. (2015), https://doi.org/10.1016/j.matdes.2014.08.060.

[25] M.G. Alberti, A. Enfedaque, J.C. Gálvez, A review on the assessment and prediction of the orientation and distribution of fibres for concrete, Compos. Part B Eng. (2018), https://doi.org/10.1016/j.compositesb.2018.05.040.

[26] E. Fonseca, A. Reguly, The use of the ultrasound measurement technique for the evaluation of mechanical properties of the ASTM A36 steels, J. Braz. Soc. Mech. Sci. Eng. 33 (2) (2011) 212–217, https://doi.org/10.1590/S1678-58782011000200013.

[27] A. Bentur, S. Mindess. Fibre reinforced cementitious composites. England: Elsevier Applied Science; 1990.

[28] F. Deng, X. Ding, Y. Chi, L. Xu, L. Wang, The pull-out behavior of straight and hooked-end steel fiber from hybrid fiber reinforced cementitious composite:

Experimental study and analytical modelling, Compos. Struct. (2018). https://doi:10.1016/j.compstruct.2018.08.066.

[29] F. Isla, G. Ruano, B. Luccioni, Analysis of steel fibers pull-out. Experimental study, Constr. Build. Mater. 100 (2015) 183–193. https://doi:10.1016/j.conbuildmat.2015.09.034.

[30] A.E. Hoerl, Fitting curves to data, in: J.H. Perry (Ed.), Chemical business handbook, McGraw-Hill, New York, 1954, pp. 55–57.

[31] Afroughsabet, Biolzi, Ozbakkaloglu, High-performance fiber-reinforced concrete: a review, J. Mater. Sci. 52 (2016) 6517–6655, https://doi.org/10.1007/s10853-016-9917-4.

[32] Abrishambaf, Pimentel, Nunes, Influence of fibre orientation on the tensile behaviour of ultra-high performance fibre reinforced cementitious composites, Cem. Concr. Res. 97 (2017) 28–40, https://doi.org/10.1016/j.cemconres.2017.03.007.